Kinetics of the Shear-Thickening Transition Observed in Dilute Surfactant Solutions and Investigated by Flow Birefringence

Jean-François Berret*

Complex Fluids Laboratory, CNRS − Cranbury Research Center Rhodia Inc., 259 Prospect Plains Road CN 7500, Cranbury, New Jersey 08512

Sandra Lerouge and Jean-Paul Decruppe

Groupe de Rhéophysique des Colloïdes, Université de Metz, 57078 Metz, France

Received September 24, 2001. In Final Form: June 19, 2002

We report on the rheo-optical properties of dilute surfactant solutions which exhibit a shear-induced thickening transition. The surfactant investigated is cetyltrimethylammonium tosylate at concentrations around 0.2 wt % in water. By comparing data obtained by rheology and rheo-optics, we first confirm that the thickening transition is associated with the transformation of the initially isotropic micellar liquid into a birefringent and strongly aligned phase. In both experiments, the transition occurs at the same critical shear rate, denoted $\dot{\gamma}_c$. Using a new treatment for the analysis of the rheo-optical data, we have been able to determine the birefringence Δn and extinction angle χ at steady state, but also as a function of the time and of the spatial coordinate in the 1 mm gap of a Couette-type shearing cell (with a spatial resolution of 15 μm). Starting from a solution in a quiescent state and applying steady shear, we provide an accurate description of the kinetics of formation of the shear-induced and viscous phase. At steady state, we observe strong variations of the flow birefringence Δn as a function of the spatial coordinates within the gap, as well as a failure of the stress-optical law. The extinction angle χ is then close to 0°, independent of the shear rate and of the spatial coordinates. The flow birefringence also exhibits rapid fluctuations around the average profiles, on a length scale comprised between 50 and 100 μm. These fluctuations are interpreted as shear bands of enhanced and reduced birefringence, a result which suggests a strongly inhomogeneous and instable shear flow in the shear-induced phase.

I. Introduction

When submitted to steady deformation rates, many complex fluids such as surfactant and block copolymer solutions, microemulsions, and colloidal dispersions exhibit a rheological transition.[1] In shear flow, rheological transitions manifest themselves by some anomaly in the shear stress versus shear rate behavior. Despite a broad literature on the rheophysics of complex fluids, these transitions are still ill understood. One of the most puzzling rheological transitions reported so far is the shear-thickening phenomenon observed in dilute or highly dilute surfactant solutions. These dilute surfactant solutions have a zero-shear viscosity very close to that of the solvent (water), and no apparent viscoelasticity is observed. However, in steady shear and above a critical strain rate denoted $\dot{\gamma}_c$, the shear viscosity increases.[2−15] The features of the shear-thickening transition vary from one surfactant system to another. However, all systems have in common the following characteristics. Shear-thickening occurs for surfactants that self-assemble into cylindrical micelles. As polyelectrolytes, the micelles are electrostatically charged. When samples are sheared above $\dot{\gamma}_c$, an induction time (t_{Ind}) is necessary to induce the more viscous state. It has been reported[2,4,10,13] that t_{Ind} increases considerably when the applied shear rate approaches $\dot{\gamma}_c$ (keeping $\dot{\gamma} > \dot{\gamma}_c$). In the shear-induced state, the solutions are birefringent[3,5] and simultaneously exhibit a strongly anisotropic scattering in light[16] and neutron[5,6,17−20] experiments. This anisotropy is compatible with the strong alignment of the shear-induced structure in the flow. The shear stress versus shear rate curve determined experimentally depends on the geometry of shearing cell, as well as on

* To whom correspondence should be addressed. E-mail: jeanfrancois.berret@us.rhodia.com.

(1) Larson, R. G. *The Structure and Rheology of Complex Fluids*; Oxford University Press: New York, 1999.
(2) Hoffmann, H.; Platz, G.; Rehage, H.; Schorr, W.; Ulbricht, W. *Ber. Bunsen-Ges. Phys. Chem.* **1981**, *85*, 255.
(3) Wunderlich, I.; Hoffmann, H.; Rehage, H. *Rheol. Acta* **1987**, *26*, 532.
(4) Wunderlich, A. M.; Brunn, P. O. *Colloid Polym. Sci.* **1989**, *267*, 627.
(5) Hofmann, S.; Rauscher, A.; Hoffmann, H. *Ber. Bunsen-Ges. Phys. Chem.* **1991**, *95*, 153.
(6) Schmitt, V.; Schosseler, S.; Lequeux, F. *Europhys. Lett.* **1995**, *30*, 31.
(7) Oda, R.; Panizzza, P.; Schmutz, M.; Lequeux, F. *Langmuir* **1997**, *13*, 6407.
(8) Boltenhagen, P.; Hu, Y.; Matthys, E. F.; Pine, D. J. *Phys. Rev. Lett.* **1997**, *79*, 2359.
(9) Hartmann, V.; Cressely, R. *Europhys. Lett.* **1997**, *40*, 691.
(10) Boltenhagen, P.; Hu, Y.; Matthys, E. F.; Pine, D. J. *Europhys. Lett.* **1997**, *38*, 389.
(11) Hu, H. T.; Boltenhagen, P.; Pine, D. J. *J. Rheol.* **1998**, *42*, 1185.
(12) Hu, Y. T.; Boltenhagen, P.; Matthys, E.; Pine, D. J. *J. Rheol.* **1998**, *42*, 1209.
(13) Gamez-Corrales, R.; Berret, J.-F.; Walker, L. M.; Oberdisse, J. *Langmuir* **1999**, *15*, 6755.
(14) Truong, M. T.; Walker, L. M. *Langmuir* **2000**, *16*, 7991.
(15) Berret, J.-F.; Gamez-Corrales, R.; Lerouge, S.; Decruppe, J.-P. *Eur. Phys. J. E* **2000**, *2*, 343.
(16) Proztl, B.; Springer, J. *J. Colloid Interface Sci.* **1997**, *190*, 237.
(17) Lindner, P.; Bewerdorff, H. W.; Heen, R.; Sittart, P.; Thiel, H.; Langowski, J.; Oberthur, R. *Prog. Colloid Polym. Sci.* **1990**, *81*, 107.
(18) Berret, J.-F.; Gamez-Corrales, R.; Oberdisse, J.; Walker, L. M.; Lindner, P. *Europhys. Lett.* **1998**, *41*, 677.
(19) Oda, R.; Weber, V.; Lindner, P.; Pine, D. J.; Mendes, E.; Schlosser, F. *Langmuir* **2000**, *16*, 4859.
(20) Berret, J.-F.; Gamez-Corrales, R.; Séréro, Y.; Molino, F.; Lindner, P. *Europhys. Lett.* **2001**, *54*, 605.

10.1021/la011471h CCC: $22.00
Published on Web 00/00/0000 PAGE EST: 7.9

whether it is the shear rate or the shear stress which is applied to the solution.[8,11,12]

A remarkable property of the shear-induced phase is its flow birefringence. Flow birefringence experiments on shear-thickening surfactant solutions were pioneered by Hoffmann and co-workers almost two decades ago.[3−5] These authors have shown that in terms of shear rate, the onset of flow birefringence coincides with the increase of viscosity. The value of the birefringence Δn was found to be negative, comprised between -10^{-5} and -10^{-7} according to the concentration. The flow birefringence was essentially measured at the steady state as a function of the shear rates and under different physicochemical conditions (temperature, concentration, salinity). A very interesting result was related to the extinction angle χ, which denotes the angle made by the neutral axes of the sheared medium and the flow velocity. For several surfactant systems, the extinction angle was found to be systematically close to 0°, indicating an excellent alignment of the shear-induced structures in the flow. The data as a function of the shear rate actually revealed that χ undergoes a discontinuity at $\dot\gamma = \dot\gamma_c$, from $\chi = 45°$ (isotropic phase) to $\chi \sim 0°$ (fully aligned state). More recent measurements[7,15] have confirmed these features.

In the present paper, we report on the flow birefringence measured on the binary surfactant system cetyltrimethylammonium tosylate (CTAT)/water at concentrations around $\phi \sim 0.2\%$. In our previous reports,[13,15,18,20] we demonstrated that CTAT dilute solutions exhibit a shear-thickening transition with features in agreement with those listed previously. Here, we focus on the kinetics of formation of the shear-induced phase as a function of time and as a function of the spatial coordinates within the shearing cell. Both the birefringence Δn and extinction angle χ were resolved in time and space, using start-up experiments at $\dot\gamma > \dot\gamma_c$. The results are interpreted in terms of inhomogeneous flow, analogous to a shear-banding flow.

II. Experimental Details

Sample Preparation. The CTAT (molecular weight, 455 g/mol) was purchased from Sigma products (purity 99%) and used as received. Attempts to purify the surfactant (by precipitation in acetone) did not change noticeably the self-assembly properties nor the rheology of the solutions. For rheological and birefringence measurements, two stock solutions were prepared at concentrations of 0.16 and 0.24 wt % using water that was purified by passage through a Millipore water system. The solutions were stored for several days at constant temperature ($T = 30$ °C) for equilibration. To avoid uncontrolled shear history, the solutions were gently poured into the shearing cells.

The CTAT concentrations of 0.16 and 0.24 wt % were chosen for this work for several reasons. First, the solutions exhibit clear and well-defined shear-thickening transitions. Second, the birefringence of the shear-induced phase is strong enough to be measured. Finally, for CTAT, these concentrations are comprised between the second critical micellar concentration ϕ_{cmc2} and the overlap concentration ϕ^*. At room temperature, the second critical micellar concentration corresponding to the change in morphology of the aggregates from spherical to rodlike has been estimated at $\phi_{cmc2} = 0.04$ wt %, whereas the overlap concentration $\phi^* \sim 0.5\%$ was determined independently from transient electric birefringence,[21] fluorescence recovery,[22] and viscosity measurements.[13] In the concentration range put under scrutiny in this work, around 0.2 wt %, the CTAT aggregates can be described as short rodlike micelles, of average length shorter than the intermicellar distance (dilute regime).

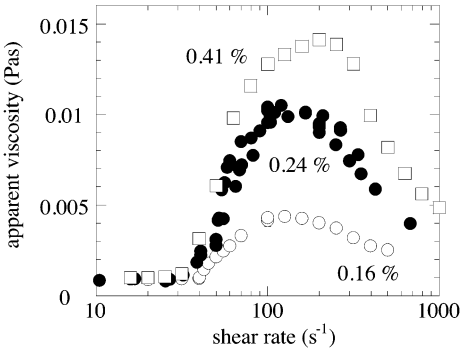

Figure 1. Steady shear viscosity as a function of the applied shear rate for cetyltrimethylammonium tosylate aqueous solutions at concentrations $\phi = 0.16\%$, 0.24%, and 0.41% and ambient temperature. The critical shear rate is defined by the onset of shear thickening. For the three solutions, $\dot\gamma_c$ is found around 40 s^{-1} (see Table 1).

Rheology. All rheological measurements were made using a Rheometrics fluid spectrometer (RFS II) equipped with a Couette configuration with controlled shear rate (outer diameter, 34 mm; gap, 1 mm; the outer geometry rotates). We recently gave a detailed account of the complex transient rheology of CTAT dilute solutions,[15] and the interested reader should refer to this paper. Here, we are dealing with the flow behavior at steady state and rheology is used as a characterization method. Figure 1 displays typical flow curves for CTAT dilute solutions below the overlap concentration.[13] The apparent viscosity has been measured as a function of the shear rate at concentrations of 0.16, 0.24, and 0.41 wt %. As reported previously,[13,15,18,20] the shear-thickening transition occurs here continuously (in applied strain mode) and the critical value $\dot\gamma_c$ is independent of the surfactant concentration. For the three solutions investigated, we found $\dot\gamma_c \sim 35$ s^{-1}. Note also in Figure 1 that the higher the concentration, the stronger the effect of thickening.

Flow Birefringence. Flow birefringence was carried out using an home-built optical device that was described in detail in ref 23. The shearing cell is a Couette cell of height $h = 30$ mm and of gap $e = 1$ mm. The inner cylinder of radius $R_1 = 24$ mm rotates. The flow birefringence has been determined by transmission using either a laser beam or an extended monochromatic light source. In both cases, the polarized light propagates along the vorticity direction of the Couette cell, that is, perpendicular to the plane defined by the velocity $\mathbf{v}$ and the velocity gradient $\nabla\mathbf{v}$ (Figure 2a). Let y be the spatial coordinates of the fluid in the gap: $y = 0$ at the outer radius and $y = e = 1$ mm at the inner radius. In steady shear, the outcoming light transmitted by the CTAT solutions was found to depend both on the time and on the spatial coordinate. We thus write the transmitted intensity of the form

$$I_\theta(y,t) = \frac{I_0}{2}\sin^2\left(\frac{\delta(y,t)}{2}\right)\sin^2[2(\chi(y,t)+\theta)] \qquad (1)$$

where I_0 is the incident and linearly polarized light intensity and θ is the angle made by the polarization of the incident beam with the flow velocity (Figure 2b). The phase angle or retardance $\delta(y,t)$ is related to the birefringence by

$$\delta(y,t) = \frac{2\pi h}{\lambda}\Delta n(y,t) \qquad (2)$$

Equations 1 and 2 assume explicitly that the extinction angle $\chi(y,t)$ and the birefringence $\Delta n(y,t)$ depend on y and t.

Method 1. Using the He−Ne laser beam (wavelength, 6328 Å), χ and Δn are measured in the steady flow only (no transient). The quantities represent the state of the flow birefringence at the center of the gap ($y = 0.5$). They are averaged over time and over the size of the laser beam (∼200 μm). The extinction angle is determined by rotating simultaneously the polarizer and

(21) Narayanan, J.; Mendes, E.; Manohar, C. *J. Phys. Chem.* **1996**, *100*, 18524.
(22) Narayanan, J.; Urbach, W.; Langevin, D.; Manohar, C.; Zana, R. *Phys. Rev. Lett.* **1998**, *81*, 228.
(23) Decruppe, J.-P.; Hocquart, R.; Wydro, T.; Cressely, R. *J. Phys. France* **1989**, *50*, 3371.

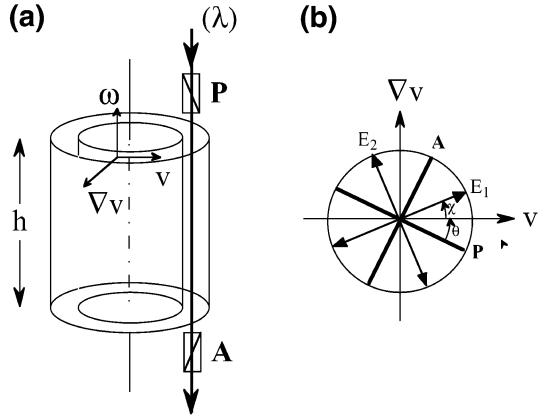

Figure 2. (a) Schematic representation of the flow birefringence device used in the present work. The shearing cell is a Couette of height $h = 30$ mm and of gap 1 mm. The inner cylinder of radius 24 mm rotates. The flow birefringence has been measured by transmission using a laser beam (wavelength, 6328 Å) or an extended monochromatic light source. The polarized light propagates along the vorticity direction of the cell. P and A stand for polarizer and analyzer. (b) In the plane defined by the velocity **v** and the velocity gradient ∇**v**, the orientations of the neutral axes of the sheared medium (E1, E2) with respect to the flow velocity determine the extinction angle χ. For an isotropic medium, $\chi = 45°$.

analyzer in order to minimize the transmitted intensity, corresponding to $\theta = \chi$ in eq 1. The retardance δ and thus the birefringence Δn through eq 2 are obtained by the Sernamont method with an accuracy of $\pm 10^{-7}$.

Method 2. The use of a monochromatic extended light beam is usually restricted to experiments aimed at the visualization of the sheared solution. In this case, a parallel light beam of diameter much larger than the gap of the Couette is sent along the vorticity direction. The transmitted light is recorded on a CCD camera using 384 × 256 pixels (spatial resolution, 15 μm/pixel) which provides an image of the sheared solution. Typical exposure times are of the order of a millisecond. An example of a photograph of a CTAT solution at 0.24 wt % taken under steady shear ($\dot{\gamma}$= 80 s^{-1}) is shown in Figure 3a. Although bands of different intensities might be visible, on average the transmitted intensity is found to decrease from the inner to the outer cylinder. To analyze these data more quantitatively, we have digitized the photographs obtained via the CCD camera along a radial line noted [AB] in Figure 3a. Figure 3b shows the results of the digitization and confirms the decrease of the transmitted intensity from R_1 ($y = 1$) to R_2 ($y = 0$). In this paper, we will use systematically the digitized photographs of the gap under cross polarizers to explore the transient and steady birefringence of the shear-induced phase of CTAT dilute solutions. One important point should be mentioned here. The angle θ between the polarizer/analyzer and the velocity field at the point of observation in Figure 3a is fixed at a value different from χ; otherwise, according to eq 1, the field of observation would appear entirely dark. To separate the contributions of Δn and of χ in the transmitted intensity, we have performed experiments using different θ configurations, for example, $\theta = 22.5°$ and $\theta = 45°$.[24] In a start-up experiment, photographs of the solution under shear were taken every second after the inception of shear, yielding a set of data at $\theta = 22.5°$. Once the steady state is reached, the rotation of the cell is stopped and the sample is let free to relax to its equilibrium state. The unsheared solutions are not birefringent. The same start-up experiment is then repeated at $\theta = 45°$. The ratio of the two intensities $I_{\theta=22.5°}(y,t)/I_{\theta=45°}(y,t)$ at a time t allows one to reconstruct the spatial dependence of the extinction angle. From eq 1, one gets

$$\frac{I_{\theta=22.5°}(y,t)}{I_{\theta=45°}(y,t)} = \frac{1}{2}(1 + tg[2\chi(y,t)])^2 \qquad (3)$$

To measure the space and time dependencies of the flow birefringence $\Delta n(y,t)$, another optical arrangement has been used.

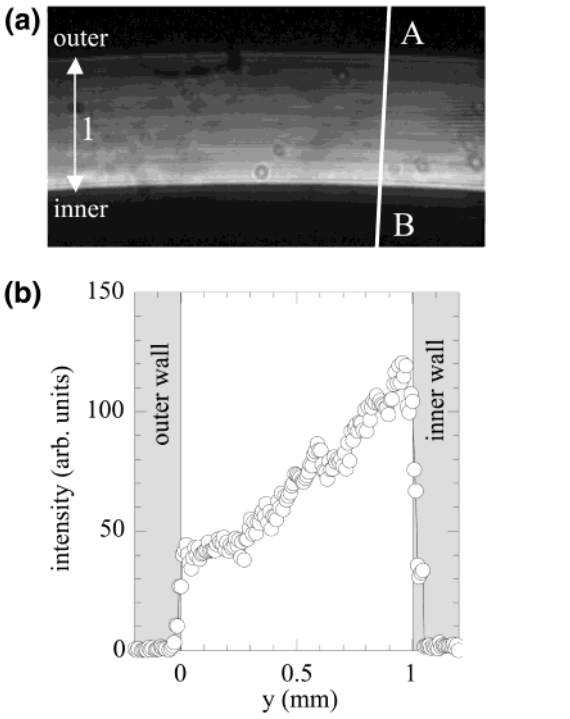

Figure 3. (a) Typical photograph of the 1 mm gap showing the light transmitted by the sheared fluid under crossed polarizers. The intensity is recorded on a CCD camera using 384 × 256 pixels, with a spatial resolution of 15 μm/pixel. The sample here is a CTAT solution at 0.24 wt % and $\dot{\gamma} = 80\ s^{-1}$. (b) Result of the digitization of the previous photograph along the line [AB], this line being shown in (a). y, the spatial coordinate of the fluid within the gap, varies between $y = 0$ (outer radius) and $y = 1$ mm (inner radius).

The linear polarizer and analyzer in the previous experiment were replaced by circular ones. Using in addition quarter-wave plates oriented at 45° with respect to the polarizer and analyzer, the transmitted intensity does not depend on the orientation of the medium under shear:[24]

$$I_c(y,t) = I_0' \sin^2\left(\frac{\delta(y,t)}{2}\right) \qquad (4)$$

where the retardance $\delta(y,t)$ has the same definition as for linear polarized light (eq 2). Note that in this case, the incident intensity I_0' is different from that in eq 1. $\Delta n(y,t)$ is then calculated according to

$$\Delta n(y,t) = \frac{\lambda}{\pi h} \arcsin\sqrt{\frac{I_c(y,t)}{I_0'}} \qquad (5)$$

III. Flow Birefringence Results and Analysis

III.1. Flow Birefringence at the Stationary State.

Figure 4 shows the shear rate dependencies of the birefringence Δn and of the extinction angle χ for the 0.16 wt % CTAT solution. At rest and below $\dot{\gamma}_c = 35 \pm 5\ s^{-1}$, the sheared solution exhibits no birefringence. Above $\dot{\gamma}_c$, there is an abrupt increase (in absolute value) of the birefringence from $\Delta n = 0$ to $\Delta n = -6 \times 10^{-7}$, while in the meantime χ goes to an angle close to zero. As the shear rate is further increased, Δn levels off for rates above 100 s^{-1}, the extinction angle remaining unchanged and close to 0°. In the shear-thickening regime, we found $\chi = \chi_{ST} = 0.7 \pm 0.3$.[15] It is important to note at this point that the

(24) Lerouge, S.; Decruppe, J. P.; Berret, J.-F. *Langmuir* **2000**, *16*, 6464. Lerouge, S. Ph.D. Thesis, Université de Metz, Metz, France, 2000, unpublished.

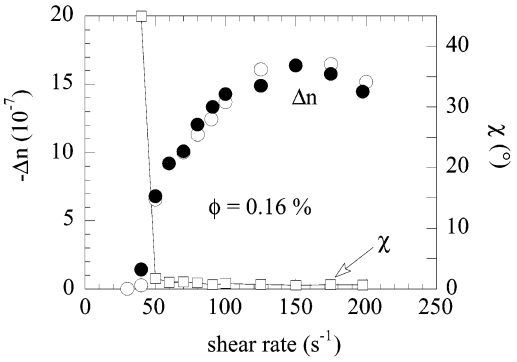

Figure 4. Shear rate dependencies of the flow birefringence Δn (left scale) and extinction angle χ (right scale) obtained for a CTAT/H_2O solution at 0.16 wt %. Note the abrupt changes of both quantities at the critical shear rate $\dot{\gamma}_c = 35 \pm 5\ s^{-1}$. The two series of data points for Δn correspond to the two different techniques described in the Experimental Section, the Sernamont technique (empty circles) and the digitization method (closed circles).

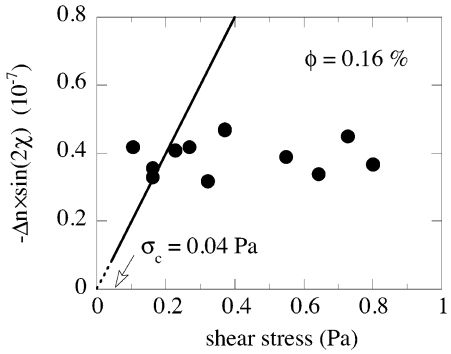

Figure 5. Test of the stress-optical law for a CTAT solution at 0.16 wt %. The product $-\Delta n \sin 2\chi$ is plotted versus the shear stress using data of Figures 1 and 4. The straight line is calculated from eq 6 with a stress-optical constant $C = -1 \times 10^{-7}$.

phenomenon of shear-induced birefringence is fully reversible. Once the shearing is ceased, the solution returns to an isotropic nonbirefringent state. The negative sign of the birefringence is discussed in the next section. In Figure 4, we also compare data obtained by the Sernamont technique (empty circles) and by the digitization method (closed circles). As explained in the Experimental Section, only the relative value of Δn is obtained with the digitization technique. Therefore, we had to multiply the data by a constant in order to adjust them to the absolute values of Δn. Both sets of data are in excellent agreement.

The Δn and χ data of Figure 4, combined with the rheological data of Figure 1, allow us to check the validity of the stress-optical law for this type of fluids. Since the flow birefringence shows up only in the shear-thickening range, this can be done only above $\dot{\gamma}_c$. The stress-optical rule is a relationship that links the refractive index tensor and the shear stress tensor through a constant C, the stress-optical coefficient. It reads

$$\Delta n \sin 2\chi = 2C\sigma$$
$$\Delta n \cos 2\chi = CN_1 \qquad (6)$$

where σ and N_1 are the shear stress and the first normal stress difference, respectively. In Figure 5, we have plotted the product $\Delta n \sin 2\chi$ versus σ for the 0.16 wt % CTAT solution. In the shear-thickening regime, with increasing shear rate, the product $\Delta n \sin 2\chi$ is found to be constant

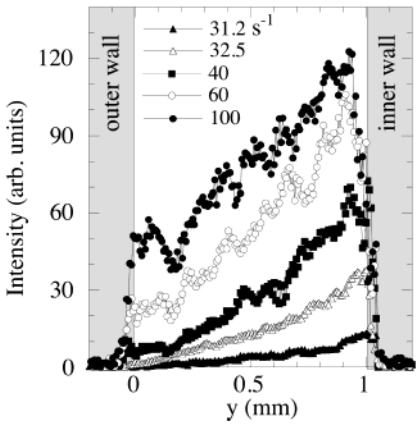

Figure 6. Steady-state intensity profiles obtained for a CTAT solution at 0.24 wt % as a function of the spatial coordinate y. $y = 0$ and $y = 1$ correspond to the outer and inner cylinder of the Couette cell, respectively. The profiles were derived by digitizing photographs taken at different shear rates: 31.2, 32.5, 40, 60, and 100 s^{-1}.

Table 1. List of the CTAT Solutions Investigated in This Work, Together with Some Experimental Quantities Derived from the Flow Birefringence Experiments

	experimental technique	$\dot{\gamma}_c$ (s^{-1})	$\dot{\gamma}$ (s^{-1})	t_{Ind} (s)	t_{Sat} (s)
CTAT/H_2O	rheology	40 ± 5			
0.16 wt %	flow birefringence	35 ± 5	100	11 ± 1	35 ± 1
CTAT/H_2O	rheology	35 ± 5			
0.24 wt %	flow birefringence	30 ± 1	40	25 ± 3	120 ± 3
			60	10 ± 1	38 ± 2
			80	7 ± 1	22 ± 1
			100	3 ± 1	14 ± 1
CTAT/H_2O 0.41 wt %	rheology	35 ± 5			

and independent of the measured stress. As a comparison, we have also plotted in Figure 5 the first relationship of eq 6 using for the stress-optical constant $C = -1 \times 10^{-7}$.[25,26] Clearly, the stress-optical law is not applicable in the thickening regime. It will be argued in the following that this is due to the fact that the shear flow is not homogeneous.

Figure 6 displays the intensity transmitted by a CTAT solution at 0.24 wt % under shear as a function of the spatial coordinate y. We recall that $y = 0$ and $y = 1$ correspond to the outer and inner cylinder, respectively. The profiles in Figure 6 were obtained by the digitization technique, from pictures of the gap taken in the stationary state between 31.2 and 100 s^{-1}. The light was polarized linearly, and the angle θ between the flow velocity and the ensemble polarizer−analyzer was $\theta = 45°$. At shear rates below and equal to 30 s^{-1}, the fluid is not birefringent and the digitized intensity is identically zero. For the 0.24 wt % solution, the first nonzero birefringence has been detected at 30.6 s^{-1}. This result agrees well with the rheological behavior of Figure 1 (see also Table 1). Moreover, as for the 0.16 wt % solution, the sample at 0.24 wt % displays an extinction angle close to 0°, at all distances y within the gap and at all shear rates. This latter result implies that the transmitted intensities in Figure 6 reflect directly the flow birefringence (through eqs 1 and 2). Assuming in eq 1 that the angle χ is independent of y and that the phase angle δ is small compared to unity, one gets $\Delta n(y) \sim I(y)^{1/2}$. $\Delta n(y)$ can thus be calculated as a function of y at each shear rate and

(25) Shikata, T.; Dahman, S. J.; Pearson, D. S. *Langmuir* **1994**, *10*, 3470.
(26) Humbert, C.; Decruppe, J. P. *Colloid Polym. Sci.* **1998**, *276*, 160.

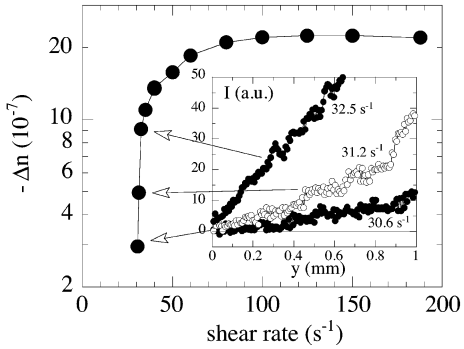

Figure 7. Shear rate evolution of the flow birefringence Δn for a 0.24 wt % CTAT solution. The use of a semilogarithmic scale aims to emphasize the behavior close to the critical shear rate, $\dot{\gamma}_c = 30\ s^{-1}$. Inset: Intensity profiles at shear rates $\dot{\gamma} =$ 30.6, 31.2, and 32.5 s^{-1}. Once the shear-induced state is initiated, it spreads over the whole gap of the cell. No regime of coexisting states (isotropic and birefringent) could be detected.

fitted using a linear dependence, according to

$$\Delta n(y) = [\Delta n(y{=}1) - \Delta n(y{=}0)]\left(\frac{y}{e}\right) + \Delta n(y{=}0) \quad (7)$$

where $\Delta n(y{=}1)$ and $\Delta n(y{=}0)$ are the values of the birefringence at the outer and inner cylinder, respectively. The slope in eq 7 $[\Delta n(y{=}1) - \Delta n(y{=}0)]/e$ is large, typically of the order of the average value of Δn. In all cases, the variation of the birefringence between the two cylinders is greater than the variation of the shear stress resulting from the curvature of the shearing cell (here $\Delta\sigma/\sigma \sim 0.08$). Note also that at a high shear rate, the profiles exhibit local fluctuations of birefringence as a function of y. As discussed in the section dedicated to the transient birefringence, these fluctuations can be viewed as shear bands of enhanced (bright) or of reduced (dark) birefringence.

One question in these experiments was crucial to us: how does the flow birefringence behave close to the critical shear rate $\dot{\gamma}_c$? Or, is there a range of shear rates over which a dark and a birefringent band coexist? The answer is no. Figure 7 displays the shear rate evolution of Δn for the 0.24% CTAT solution. The flow birefringence increases rapidly above $\dot{\gamma}_c$ and saturates in the shear-thinning regime (see Figure 1). In the inset are represented the intensity profiles for the shear rates $\dot{\gamma} = 30.6$, 31.2, and 32.5 s^{-1}, that is, slightly above $\dot{\gamma}_c$. As shown in the inset, already at 31.2 s^{-1}, the solution is birefringent over the whole field of observation. At 30.6 s^{-1}, only 4/5 of the gap displays a nonzero transmitted intensity. We attribute this result to the lack of sensitivity of the detector, rather than to a coexistence of phases. From the data shown in Figure 7, we conclude that once the shear-induced state is initiated, it spreads over the whole gap of the cell, and no regime of coexisting states isotropic/birefringent is detected.

III.2. Time-Resolved Flow Birefringence. Figure 8a,b illustrates the development of the birefringence (expressed in terms of the transmitted intensity) as a function of the time in start-up experiments. Shear rates are 60 s^{-1} and $\dot{\gamma} = 100\ s^{-1}$, respectively, and we focus here on the 0.24% CTAT solution. Several time regimes are distinguished in Figure 8. Up to the induction time denoted t_{Ind} (see Table 1), no birefringence can be detected. Above t_{Ind}, flow birefringence shows up at the vicinity of the inner cylinder. The intensity increases progressively and spreads out in the gap. At the end of this regime, occurring at the saturation time t_{Sat}, the whole gap appears birefringent

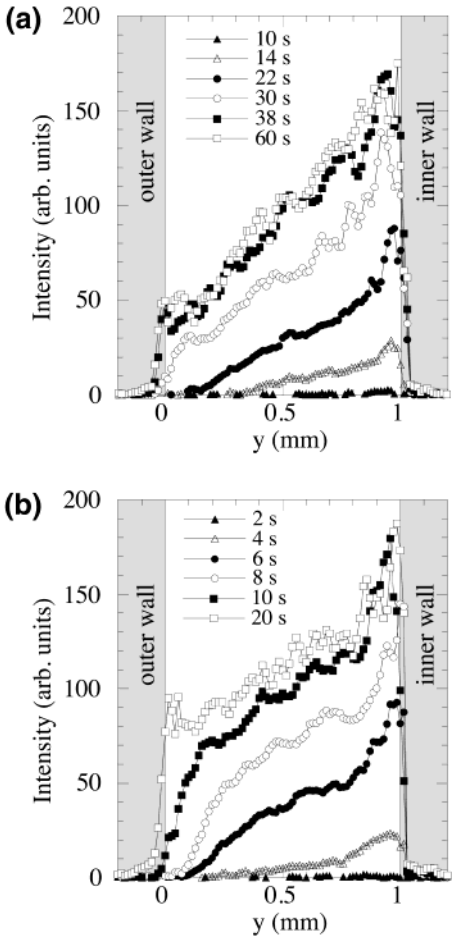

Figure 8. (a,b) Transient behavior of the flow birefringence, illustrated in terms of the transmitted intensity, as a function of the time in a step shear rate experiment. Shear rates are 60 s^{-1} in (a) and $\dot{\gamma} = 100\ s^{-1}$ in (b). The induction and saturation times t_{Ind} and t_{Sat} for these experiments are listed in Table 1.

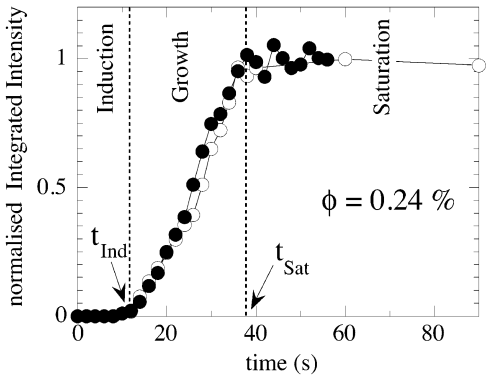

Figure 9. Time evolution of the normalized integrated intensity in step shear rate experiments at 60 s^{-1}. The experiments were performed on two different samples of the same 0.24 wt % CTAT stock solution (full and empty symbols). The induction, growth, and saturation time regimes are indicated.

between crossed polarizers. The kinetics of growth of the shear-induced phase is more rapid at 100 s^{-1} (Figure 8b) than at 60 s^{-1} (Figure 8a). The time regimes discussed above are shown in more detail in Figure 9, which displays the normalized integrated intensity as a function of time, for two runs at 60 s^{-1}. This start-up experiment was performed on two different samples of the same 0.24 wt % CTAT stock solution, and the agreement between the two sets of data attests to the reproducibility of the experimental procedure. The induction, growth, and

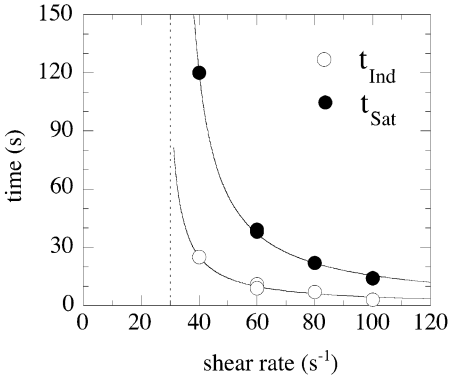

Figure 10. Shear rate dependence of the two characteristic times t_{Ind} and t_{Sat} above $\dot{\gamma}_c$. Data are for CTAT at $\phi = 0.24\%$. The continuous lines are best fit calculations using eq 8.

saturation time regimes are indicated. For this sample, one has $t_{Ind} = 10 \pm 1$ s and $t_{Sat} = 38 \pm 2$ s (Table 1). In Figure 10, we investigate the shear rate evolution of these two characteristic times above $\dot{\gamma}_c$. As $\dot{\gamma}$ decreases, t_{Ind} and t_{Sat} exhibit an apparent divergence, according to

$$t_{Ind,Sat} \sim \frac{1}{\dot{\gamma} - \dot{\gamma}_c} \tag{8}$$

Equation 8 is shown by continuous lines in Figure 10 for t_{Ind} and t_{Sat}, using the critical shear rate $\dot{\gamma}_c$ as an adjustable parameter. We found $\dot{\gamma}_c = 27$ and 31 s^{-1}, respectively, in agreement with previous determinations. It should be emphasized that due to the small number of data points in Figure 10, a power law dependence of the form $t_{Ind,Sat} \sim \dot{\gamma}^{-m}$ can provide equally good fits, and for the CTAT solution at 0.24 wt %, the exponent of the scaling would be $m \sim 2.2$. Power law dependencies for the induction times have been found repeatedly in the literature.[2,10,16] The advantage of eq 8 over the power law dependence is that it emphasizes the existence of a critical shear rate or shear stress necessary to trigger the transition.

As already mentioned, at the stationary state in the shear-induced regime, the transmitted light profiles exhibit fluctuations as a function of the distance y in the gap. To illustrate these fluctuations more clearly, we have plotted in Figure 11 the relative intensity $[I(y,t) - \langle I(y)\rangle_t]/\langle I(y)\rangle_t$ for different times after the inception of the shear, where $\langle I(y)\rangle_t$ denotes the time-averaged intensity. $\langle I(y)\rangle_t$ was calculated by summing profiles taken at different times in the stationary state, and this average was used to derive the linear dependence of the birefringence discussed previously in eq 7. The data in this figure are taken from the start-up experiment already shown in Figure 8a ($\phi = 0.24$ wt %, $\dot{\gamma} = 60$ s^{-1}). The relative intensities for times comprised between 46 and 56 s after the inception of shear exhibit spatial fluctuations of about ±20% around the average values (indicated by arrows). These fluctuations can be interpreted as shear bands of enhanced (bright) or of reduced (dark) birefringence. As shown by the succession of the five profiles, these bands are not fixed as functions of time or space but rather fluctuate rapidly under shear. At $\dot{\gamma} = 60$ s^{-1}, the characteristic length scale of these fluctuations (typically the average width of the bands) is ∼50−100 μm.

III.3. Spatially Resolved Flow Birefringence. One of the advantages of the experimental procedure based on the digitization of the transmitted intensity is that one can have access simultaneously to the extinction angle χ and to the flow birefringence Δn as a function of the time (in a start-up experiment) and as a function of the spatial

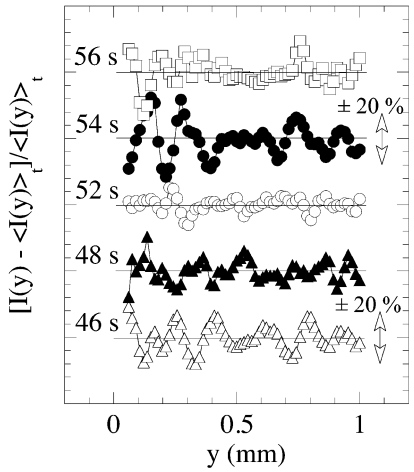

Figure 11. Relative intensity $[I(y,t) - \langle I(y)\rangle_t]/\langle I(y)\rangle_t$ as a function of the distance y within the gap for different times after the inception of the shear. The time-averaged intensity $\langle I(y)\rangle_t$ was calculated by summing profiles at different times in the stationary state. The data are taken from the start-up experiment shown in Figure 8a ($\phi = 0.24$ wt % and $\dot{\gamma} = 60$ s^{-1}). The transmitted intensity exhibits fluctuations of relative amplitude of ±20% around the average profiles.

coordinate y. As described in the Experimental Section, we have investigated the CTAT solution at 0.16 wt % in start-up experiments at 100 s^{-1} using three different experimental configurations. The first and second experiments were carried out with linearly polarized light with an angle θ between the plane of polarization of the incident light and the flow velocity of $\theta_1 = 22.5°$ and $\theta_2 = 45°$, respectively. Transmitted intensities of the sheared solution were recorded every second after the inception of shear, and $\chi(y,t)$ was calculated from the ratio of the two intensities, according to eq 3. In a third experiment, we used circular polarized light to derive the time- and space-resolved flow birefringence, using then eq 5. For CTAT/H_2O at 0.16 wt %, the induction and saturation times are $t_{Ind} = 11 \pm 1$ s and $t_{Sat} = 35 \pm 1$ s (see Table 1). In the gap of 1 mm, five points denoted A, B, C, D, and E have been selected, corresponding to the coordinates $y_A = 0.04$ mm, $y_B = 0.2$ mm, $y_C = 0.4$ mm, $y_D = 0.6$ mm, and $y_E = 0.8$ mm, respectively. In the inset of Figure 12a, there is a representation of the gap of the Couette with the positions of these five points with respect to the inner and outer cylinders. Figure 12a shows the time evolution of the extinction angle χ for B(y_B=0.2), C(y_C=0.4), D(y_D=0.6), and E(y_E=0.8). The first reliable measurement starts 4 s after the shear-induced phase appears, that is, 15 s after the inception of the flow. Already at that time, the solution displays a noticeable alignment, with $\chi \sim 25°$. $\chi(y,t)$ is found to decrease rapidly to its stationary value. Note that the uncertainty on χ is rather large, of the order of ±4°. Taking that into account, the stationary values are in agreement with those measured directly ($\chi_{Stat} = 0.7°$, see Figure 4). There are two remarkable results in Figure 12a. First, the decrease of the extinction angle from 45° (for $t < t_{Ind}$) to its stationary value is uniform through the gap. Second, the stationary angle is reached well before the saturation of the birefringence, at $t_{Sat} = 35$ s. The overall dependence of $\chi(t)$ measured for this CTAT solution at the shear-thickening transition is very similar to that obtained by light scattering experiments by Protzl and Springer on the C_{14}DMAO/SDS system.[16]

Figure 12b displays the time dependence of the flow birefringence $\Delta n(y,t)$ for the five selected points A(y=0.04), B(y=0.2), C(y=0.4), D(y=0.6), and E(y=0.8). The absolute

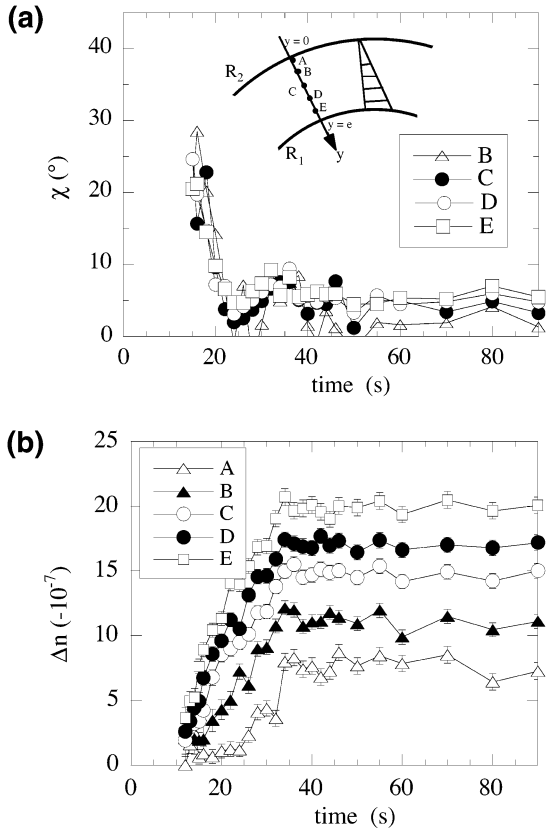

Figure 12. (a,b) Time dependence of (a) the extinction angle $\chi(y,t)$ and of (b) the flow birefringence $\Delta n(y,t)$ at different points in the gap of the Couette cell. Five points denoted A, B, C, D, and E have been selected, corresponding to the coordinates $y_A = 0.04$ mm, $y_B = 0.2$ mm, $y_C = 0.4$ mm, $y_D = 0.6$ mm, and $y_E = 0.8$ mm, respectively. They are shown in the inset of (a). The data are from a start-up experiment at 100 s^{-1}, performed on a CTAT aqueous solution at 0.16 wt %. Note that the decrease of the extinction angle from 45° to its stationary value is uniform throughout the gap.

scale for $\Delta n(y,t)$ has been obtained by comparing the transmitted intensity in the middle of the gap (points C and D) with the value measured by the Sernamont method. As shown by Figure 12b, the kinetics of growth of the shear-induced phase is more rapid close to the inner cylinder (point E) than close to outer cylinder (point A). However, the saturation in Δn occurs simultaneously through the gap. In the next section, we summarize the kinetics of growth derived from the time and space dependencies of χ and Δn.

IV. Discussion

This section aims to summarize some experimental findings known on the shear-thickening transition and to complement them by the present birefringence results. For this, several aspects will be discussed:

(1) the shear-induced changes of aggregation morphology at the transition,

(2) the origin of the flow birefringence in CTAT dilute surfactant solutions, and

(3) the kinetics of the transition as seen by flow birefringence.

IV.1. Shear-Induced Changes of Morphology. Using small-angle neutron scattering, we have demonstrated recently[20] that the shear-thickening transition in CTAT dilute solutions is accompanied by a growth of the micellar aggregates. These results have been found by comparing the scattering from solutions at rest and under shear. To this aim, the scattering structure factor was investigated as a function of the surfactant concentration and as a function of the shear rate. In CTAT dilute solutions, the structure factor arises from the electrostatic interactions between micelles,[13] and it exhibits a well-defined maximum at a wave vector $q_{Max} \sim 0.01$ Å^{-1}. Below ϕ^*, there is a systematic shift of the structure factor peak to lower wave vectors (~40%), indicating that from short cylindrical aggregates at rest, the micelles become elongated and wormlike under shear. Neutron scattering however did not allow us to estimate the average length of the micelles under shear.

There is a second indication of the wormlike micellar character of the shear-induced phase: its viscoelasticity. CTAT dilute solutions at rest or below the transition are purely viscous. The viscoelasticity of the shear-induced phase is observed in stop-flow experiments. In CTAT, as well as in other thickening surfactant systems,[2,3,5,7,15,18] when the flow is stopped from the high shear rate regime, the shear stress is found to relax exponentially to zero in a characteristic time. For CTAT in H_2O, this time is of the order of 1 s, and in CTAT with D_2O, this time is of the order of 10 s. The stress relaxation mechanism is complex and probably combines disentanglement and scission events (without recombination[27]) of the micellar chains.

IV.2. Origin of the Flow Birefringence. Another fundamental property of the shear-induced phase is its flow birefringence. In flexible macromolecules such as wormlike micelles, birefringence arises primarily from the anisotropy of the polarizability tensor of the micellar monomer (Kuhn segment) from which the whole chain is made. The birefringence is the sum of the intrinsic birefringence which comes from the anisotropy of the medium itself and the form birefringence which takes into account the anisotropy of the macromolecules in solutions.[24] For flexible chains, calculations are more complicated than for rigid ellipsoids since the deformation of the chains will superimpose to the orientation effect. The stress-optical law usually gives a correct framework for the dependencies of the refractive index tensor as a function of the stress tensor (eq 6). For wormlike micelles, the stress-optical constant C can be expressed as[25,26]

$$C = \frac{2\pi(n^2+1)^2}{45nk_BT}\Delta\alpha \quad \text{with} \quad \Delta\alpha = \frac{2\Delta\alpha^0}{\lambda}l_p \qquad (9)$$

where n is the mean refractive index, k_B is the Boltzmann constant, $\Delta\alpha^0$ is the optical anisotropy of the polarizability of a monomer (of length $\lambda \sim 8.5$ Å), and l_p is the persistence length which is twice the length of the Kuhn segment. The negative sign for the stress-optical constant arises from that of $\Delta\alpha^0$. Shikata and co-workers,[25] and Decruppe and co-workers[24,26] have demonstrated that the stress-optical law, combined with the present definition of the constant C, is valid in semidilute wormlike surfactant solutions. Equation 9 is used to determine the persistence length of wormlike micelles. For dilute CTAT solutions however, the stress-optical law is not valid (Figure 5). There are several possible explanations for this. One is that the state of the flow in the thickening regime is nonhomogeneous, that is, characterized by a nonlinear velocity field. Nonlinear flow fields have already been observed above the thickening transition, for instance, in equimolar solutions of Ethoquad T/13-50 and sodium salicylate (NaSal/TTAA).[11,12] The velocity profiles were found to display slipping layers at the walls, most of the

(27) Cates, M. E. *Macromolecules* **1987**, *20*, 2289.

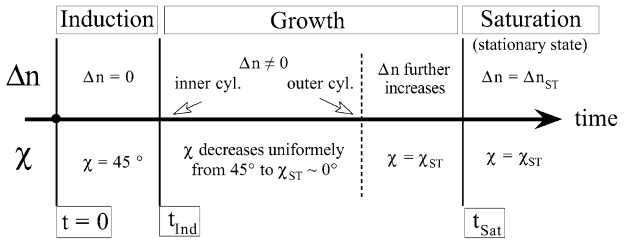

Figure 13. Summary of the kinetics of growth of the shear-induced phase in dilute CTAT aqueous solutions, as derived from the time- and space-resolved flow birefringence.

sample being in solid rotation (plug flow). From the present data, it is not possible to conclude about the nature of the flow field in the shear-induced state. It remains that the failure of the stress-optical law in CTAT systems has an important meaning: the level of the stress transmitted by the solution is not correlated to the state of orientation of the wormlike micelles seen by rheo-optical techniques. The stress measured by rheometry is much larger than the one calculated from birefringence (Figure 5).

IV.3. Kinetics of the Transition As Seen by Flow Birefringence. From the study of the time- and space-resolved birefringence, we conclude that the kinetics of the shear-thickening transition in CTAT dilute solutions occurs in three successive stages. These three regimes are identified in Figure 9 as the induction, the growth, and the saturation of the shear-induced birefringence phase. The description of this kinetics applies for all shear rates above $\dot{\gamma}_c$. In the first time regime, $t < t_{Ind}$, the birefringence is identically zero and the extinction angle χ is 45°. In the second regime, at times slightly above t_{Ind}, the micellar liquid close to the inner (rotating) cylinder becomes birefringent. This birefringence is still weak, of the order of -10^{-7}, but fills up progressively the gap of the Couette cell. During this stage, the extinction angle χ decreases to its stationary value $\chi_{ST} \sim 0°$. This decrease occurs simultaneously for all fluid layers in the gap (Figure 12a). This second stage of the kinetics is most probably the period during which the micelles undergo their unidimensional growth, from rodlike to wormlike aggregates. Once the gap is filled with the birefringent phase, there is a further and homogeneous increase of Δn up to the saturation (steady state). In the stationary regime of flow, Δn depends noticeably on the spatial coordinates in the gap. The time-averaged $\Delta n(y)$ is found to vary linearly with y at all shear rates. In addition, the birefringence exhibits short-time and short-scale fluctuations of relative amplitude of ±10% around the average profiles. These fluctuations of brightness appear actually as shear bands. The dynamic of these bands may be related to the fluctuations of the shear stress found at steady state for numerous thickening systems,[2−7,10−12,28] as well as in CTAT dilute solutions.[13,15] On the other hand, the extinction angle is constant everywhere and close to zero. These different time regimes are summarized in Figure 13.

V. Concluding Remarks

By comparing the critical shear rates obtained from rheology and from rheo-optics on CTAT dilute solutions, we have confirmed that the shear-thickening transition is associated with the transformation of the micellar liquid from an isotropic to a birefringent and strongly aligned state. For the present CTAT solutions (∼0.2 wt %), we have found flow birefringences of the order of -10^{-6} and extinction angles χ close to 0° in the shear-thickening regime. Interestingly, the alignment angle depends neither on the shear rate nor on the position in the gap where it is measured. We have been able to describe accurately the kinetics of formation of the shear-induced phase. Moreover, for the first time in shear-thickening systems, flow birefringence data have been shown simultaneously as a function of time and as a function of the spatial coordinates with a resolution of 15 μm. This has been made possible by the use of a new digitization technique of the birefringence data.

As far as the orientation of the wormlike micelles in the thickened state is concerned, the present rheo-optical results corroborate recent small-angle neutron scattering data obtained on the same materials.[20] Both techniques suggest that the shear-thickening transition is associated with a shear-induced growth of micellar aggregates of cylindrical morphology. Once the micelles have grown, in a process that remains to be clarified, the solution undergoes an instability similar to shear banding. Two rheo-optical observations suggest that the flow in the shear-thickened state is nonhomogeneous and shear banded. First, there is the large variation of flow birefringence between the inner and outer walls of the cell. This difference exceeds by far the inhomogeneity in shear stress due to the curvature of the cell. Second, there are the spatial fluctuations of the transmitted intensity on a length scale of 50−100 μm, which could indicate a multibanded instable flow.

During the course of this work, we have been aware of a paper by Cates and Candau on a plausible mechanism at the origin of the transition.[29] The speculative scenario imagined by these authors is based on the coexistence in the quiescent state of large rings (micelles closed to themselves) with open chains. The linking and delinking kinetics of the rings submitted to shear would control the thickening process, and the slow relaxations (seen in rheology) would result from the equilibrium between closed and open chains. Our small-angle neutron scattering data on CTAT quiescent solutions[13,18,20] have been interpreted so far in terms of rodlike micelles in a dilute regime of concentration ($\phi < \phi^*$). The coexistence of these micelles with large rings, or with supramolecular structures such as huge wormlike micelles or pieces of entangled network,[15] will be put under scrutiny in a forthcoming experiment.

Acknowledgment. We thank R. Gamez-Corrales and F. Molino for their help and assistance in the course of this work and for illuminating discussions.

LA011471H

(28) Bandyopadhay, R.; Basappa, G.; Sood, A. K. *Phys. Rev. Lett.* **2000**, *84*, 2022.

(29) Cates, M. E.; Candau, S. J. To appear in *Europhys. Lett.*